Journal of Applied Electrochemistry **34**: 911–918, 2004.

Cyclic voltammetric studies of carbon steel in deaerated $NaHCO_3$ solution

M.M. EL-NAGGAR
Department of Chemistry, Faculty of Science, Benha University, Benha, Egypt

Received 3 July 2003; accepted in revised form 30 March 2004

Key words: carbon steel, cyclic voltammetry, $NaHCO_3$, pre-cathodization treatment

Abstract

The voltammetric response of per-cathodic activated carbon steel electrode in deaerated 0.50 M $NaHCO_3$ solution at pH 8.72 and 25 °C at a scan rate of 25 mV s^{-1} was investigated. The influence of cycling, potential excursion and scanning rate on the anodic behavior was studied. The results revealed a specific effect of HCO_3^- ions on the overall anodic process. The complex reaction pathways involving possible competitive anodic consecutive steps and related intermediates were discussed and summarized.

1. Introduction

Study of the electrochemical and passivation behavior of iron and steel in alkaline media has attracted the attention of many researchers because of the importance of their technical applications. However, a number of published results seem to lack reproducibility. It has been suggested that the difficulties of obtaining reproducible results could disappear when prolonged cathodic activation pre-treatment is applied to the working electrode surface [1–3].

Generally, metallic iron and steel exhibit at least two main anodic peaks during anodization in alkaline solutions [3–10]. The two peaks are believed to correspond to the formation of Fe(II) and Fe(III) surface films. On the other hand, there is no such agreement regarding formation of other oxide forms such as Fe(VI) species. This situation arose due to the fact that most of the early studies [4–7] on the electrochemistry and passivation of iron and steel in alkaline solutions was performed using galvanostatic and potentiostatic techniques. More recent studies have used advanced electrochemical techniques [3, 8–10] and surface analysis of films [11–16], which provide valuable insight into the mechanistic aspects and the kinetics of dissolution and film formation. However, there is still controversy regarding the number of anodic peaks and the interpretation of the electrochemical behavior of iron and steel in alkaline solutions.

In general, the dissolution behavior of iron and steel in alkaline media is difficult to study because of the ease of formation and slow dissolution of protective layers. These effects are confounded by the numerous parameters influencing the kinetics of the anodic dissolution [17]. Further complications have been attributed to the possibility that the chemical nature of the electrolyte [18] may alter the structure of the metal/electrolyte interface, catalyze or inhibit metal dissolution and may also change the reaction path. Changes of the interface may also arise from the various intermediates and the final reaction products formed on the substrate surface. In addition to these uncertainties, the role played by the anion of the electrolyte and the cathodic pre-treatment remains unclear.

Although it was established that passivity of iron and steel in alkaline solutions is mainly associated with γ-Fe_2O_3 film formation, the exact conditions leading to the development of the passive film are not fully understood. The purpose of the present study is to verify reproducibility conditions and to explore more fully the exact conditions leading to the formation of surface films on carbon steel in $NaHCO_3$ solution. The results are intended further clarity the mechanism of film formation. Particular attention to the role of HCO_3^- ions in the overall anodic process is taken into consideration.

2. Experimental details

Carbon steel rod with the following chemical composition (in weight percent) was used: 0.260% C, 1.350% Mn, 0.040% P, 0.050% S, 0.005% Nb, 0.020% V, 0.030% Ti and balance Fe. A rod was embedded in Araldite, leaving one exposed surface of area 0.24 cm^2 as the working electrode. Electrical contact was achieved through thick copper wire soldered to the end of the rod, but not exposed to the solution. Before each experiment the electrode was successively polished with 600 and 1000 grade emery papers, subsequently degreased with acetone, and then washed with running doubly distilled water.

0.50 M $NaHCO_3$ solution was prepared from doubly distilled water and analytical grade (Merck) reagent. Deaeration of the test solution was achieved by bubbling highly pure nitrogen for 1/2 h before use.

Measurements were carried out in a three-compartment electrochemical glass cell. The auxiliary electrode was a platinum grid separated from the main compartment by fritted glass. The reference electrode was a saturated calomel electrode (SCE) with a Luggin capillary probe placed under the working electrode surface to minimize the ohmic potential drop through the cell.

Voltammetric measurements were performed using a Wenking potentioscan (type pos. 73). The cyclic voltammograms were recorded from −1.25 to +1.25 V and plotted using an X–Y recorder (Type pL 3). All tests were carried out at 25 °C.

3. Results and discussion

3.1. *Reproducibility studies*

The experimental variables were firstly examined, to establish conditions under which reproducible current–potential curves are possible. These variables included purity of the ground electrolyte, aeration and deaeration of the solution, and cathodic pretreatment of the electrode surface. It was found that deaerated 0.50 M $NaHCO_3$ solution and pre-cathodization of the carbon steel electrode for 15 min at −1.25 V produced reasonable reproducibility of the results. Apart from the pre-cathodization treatment and careful control of the experiments, the existence of excellent reproducible results indicates that the presence of HCO_3^- ions overcome most of the difficulties observed by various authors for iron and steel in alkaline solutions.

Figure 1 presents a typical reproducible cyclic voltammogram of pre-cathodic, activated carbon steel electrode in deaerated 0.5 M $NaHCO_3$ solution of pH 8.72. The voltammogram was scanned between −1.25 and +1.25 V at a rate of 25 mV s^{-1} at 25 °C. The forward half-cycle of the voltammogram consists of an initial region of hydrogen evolution (region A) followed by shoulder B. There are four successive well-defined anodic peaks (C, D, E and F), a current plateau G and a well-defined anodic peak H before oxygen evolution at I. By reversing the potential direction after oxygen evolution, the backward half-cycle of the voltammogram was obtained. It exhibited a re-oxidation current plateau J, a first cathodic peak K, a cathodic shoulder L and a second cathodic peak M at the extreme negative potential before hydrogen evolution.

In order to explain the features exhibited in Figure 1, and to define their respective roles in the mechanisms and kinetics of film formation–dissolution as well as passivation, additional studies are needed. These studies include cycling, potential excursion and potential scan rate.

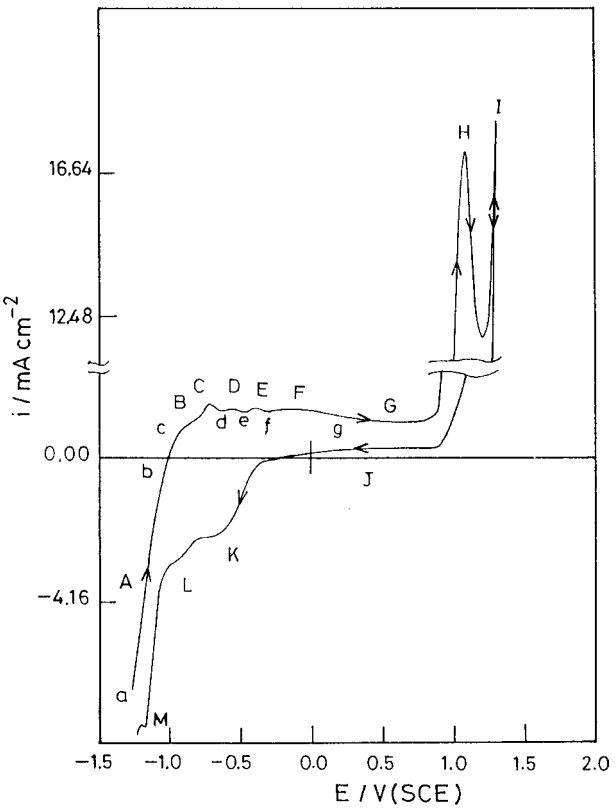

Fig. 1. Typical reproducible cyclic voltammogram obtained for carbon steel electrode in deaerated 0.50 M $NaHCO_3$ solution at a sweep rate of 25 mV s^{-1} and 25 °C.

3.2. *Effect of cycling*

Figure 2 shows three successive repeated cyclic voltammograms of the pre-cathodic activated carbon steel electrode in deaerated 0.50 M $NaHCO_3$, traced between the hydrogen and oxygen evolution potentials at a scan rate of 25 mV s^{-1} at 25 °C. The voltammograms of the second and third cycles coincide significantly. In the meantime, substantial differences are seen between them and the first cycle. The main differences between the first and second cycles may be attributed to the pre-cathodic activation treatment of the electrode surface, as summarized below:

(i) An observable increase in the anodic current density was noted over the whole potential range up to the beginning of oxygen evolution (first cycle). This behavior indicates continuous anodic dissolution.

(ii) The initial equilibrium potential at point b of the first cycle was shifted from −1.00 V to a less negative value (−0.85 V) in the second cycle, during which two pronounced effects were observed. The first was the disappearance of shoulder B and its amalgamation with the first anodic peak C. The second was the disappearance of the two anodic peaks D and E and their amalgamation with the anodic peak F.

The congruence between the traces of the second and third cycles may be taken to indicate that surface roughness effects were precluded. Hence, the overall

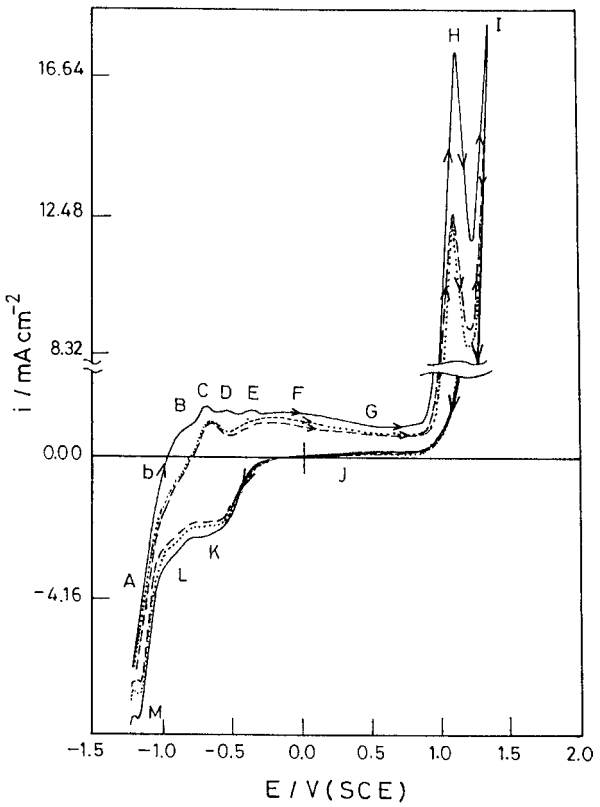

Fig. 2. Three successive sweeps for carbon steel electrode in deaerated 0.50 M $NaHCO_3$ solution at a sweep rate of 25 mV s^{-1} and 25 °C; (—) first, (····) second and (- - -) third sweep.

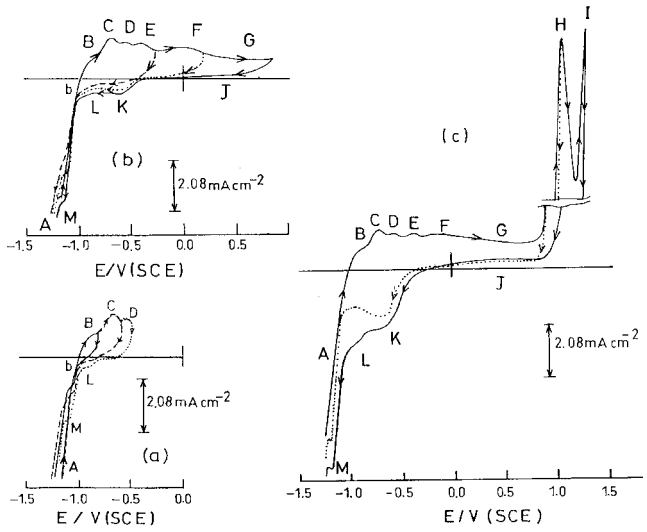

Fig. 3. Cyclic voltammograms of carbon steel electrode in deaerated 0.50 M $NaHCO_3$ solutions obtained with different reversal potentials at a sweep rate of 25 mV s^{-1} and 25 °C. a: (—) after shoulder B, (- - -) after peak C and (····) after peak D. b: (- - -) after peak E, (····) after peak F and (—) at the end of plateau G. c: (····) at the maximum of peak H and (—) complete cycle.

electrochemical processes must have been comprised of anodic and cathodic complementary processes. This indicates that the activation effects of the cathodic pretreatment disappeared completely after the first voltammetric cycle.

3.3. *Potential excursion studies*

In order to define the origin of the reduction peaks subsequent to the anodic oxidation, a number of sweep reversal experiments were preformed on the precathodic, activated carbon steel electrode. Results of these experiments are displayed in Figure 3 (a–c), from which the following points are determined:

(i) Noticeable in Figure 3a is the correspondence of the anodic shoulder B to the cathodic peak M and the shift of the hydrogen evolution reaction to more negative values. It is therefore suggested that the shoulder B is indicative of a more complex electrochemical process.

(ii) By reversing the direction of potential after the anodic peak C (Figure 3a), an additional shoulder L was noticed and a further increase in the charge of the cathodic peak M was observed. This indicates that the cathodic shoulder L is related to the peak C. The associated charge of the cathodic shoulder L is small when compared with that of the corresponding anodic peak C. This is thought to be indicative of the presence of chemical dissolution.

(iii) On reversing the potential after the two anodic peaks D and E, respectively (Figure 3a and b), no corresponding peaks were observed and the changes in the charge of shoulder L and peak M were not significant. Moreover, an initiation of peak K appeared (within experimental error). Thus, the presence of an anodic background current in the potential region of peaks D and E indicates the formation of soluble intermediate species.

(iv) According to Figure 3b, the anodic peak F corresponds to the cathodic peak K. Also seen in the figure is the appearance of a re-oxidation current plateau J and a further increase in the charge of the cathodic branch (K, L and M) is observed after potential reversal at the end of plateau G.

(v) After reversing the potential at the maximum of the anodic peak H (Figure 3c) a rise in the charge of the cathodic branch (K, L and M) is noticed. Coupled with this was the re-activation of the electrochemical oxidation process (plateau J). These effects were plausibly the result of the complete dissolution of a high valence species at the electrode surface, leaving a lower valence species on the surface.

(vi) Figure 3c shows that no new cathodic peak is observed corresponding to the anodic peak H; this is attributable to the presence of complete chemical dissolution.

3.4. *Potential scan rate studies*

Figure 4 shows the cyclic voltammograms of precathodic activated carbon steel electrodes at different scan rates ranging from 15 to 45 mV s^{-1}. Increasing the scan rate has no discernible effect on the initial

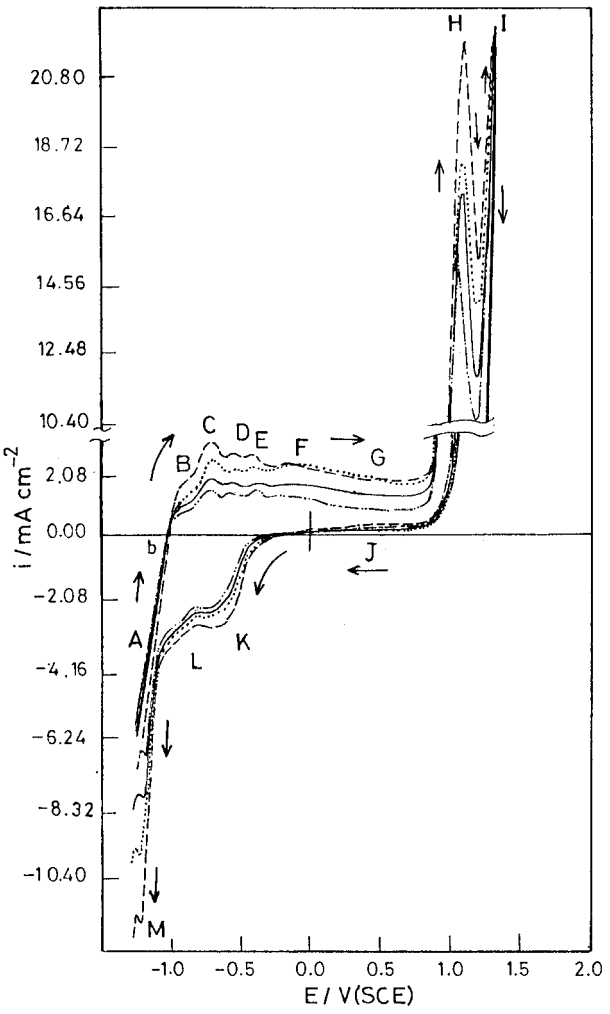

Fig. 4. Effect of different sweep rate on the cyclic voltammogram behavior of carbon steel in deaerated 0.50 M $NaHCO_3$ solutions at 25 °C; (·--·) 15, (—) 25, (····) 35 and (- - -) 45 mV s^{-1}.

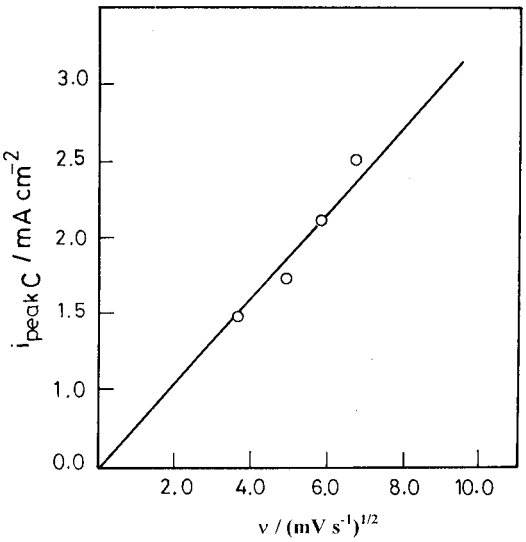

Fig. 5. Dependence of i_{peak} on the square root of the sweep rate ($\nu^{1/2}$) for the anodic peak C.

equilibrium potential (i.e. point b, −1.00 V), on the number of peaks, nor on the peak potentials. However, it appears that there is an increase in the charge of the cathodic features corresponding to the increase in current density over all the anodic features.

A plot of the current density of the first anodic peak C as a function of the square root of the scan rate is shown in Figure 5. The relationship is evidently that of a straight line passing through the origin, an attribute which implies the dominance of diffusive transport.

3.5. *Mechanisms*

To understand and interpret the mechanism of passivation of carbon steel in deaerated 0.50 M $NaHCO_3$ solution, it is necessary to first consider the basic regularities of the anodic passivation behavior of iron in NaOH in order to be able to detect the effectiveness of the $NaHCO_3$ supporting electrolyte. Such a comparison is available for iron electrodes in NaOH solutions [3, 8]. The anomalous behavior of the carbon steel as compared to the iron/NaOH system at identical pH may be attributed to the influence of the HCO_3^- ion and its catalytic effect [19].

It is of importance to point out that upon hydrolysis of $NaHCO_3$, which is a salt of a weak acid and a strong base, hydroxyl ions appear which are capable of forming a passivating oxide. $NaHCO_3$ takes preference over ordinary alkali since the hydroxyl ions used in the formation of passivating oxide are automatically replenished by hydrolysis. Moreover, the effect of $NaHCO_3$ consists in more than just increasing the concentration of hydroxyl ions needed to the formation of passivating layers. Here, there also exists a specific action of the HCO_3^- ion itself. It may have the capacity to adsorb or to form sparingly soluble compound or to participate in the elementary processes. Also, the inhibiting capacity of HCO_3^- ion was considered.

3.5.1. *Anodic oxidation*

Apart from the beginning and the end of the anodic polarization curve (see Figure 1), the anodic dissolution rate remains at a very low value with no discontinuity over a wide range of potential. This reveals that the metal was almost in the passive state. As such, the presence of HCO_3^- ions may produce an inhibiting effect.

Further inspection of the voltammogram of Figure 1 reveals that the forward half-cycle consists of four well-defined anodic regions in the potential range −0.91 to +1.25 V. These are corresponding to the following main regions:

(i) The first (active) region (−0.91 to −0.63 V), within which the shoulder B and the peak C are unmistakable.
(ii) The second (pre-passive) region (−0.63 to −0.33 V), within which peaks D and E are evident.
(iii) The third (passive) region (−0.33 to +0.88 V), within which the peak F and the plateau G are clearly noticed.

(iv) The fourth (trans-passive) region (+0.88 to +1.25 V), within which the peak H and oxygen evolution peak I are conspicuous.

Moreover, each of the above four potential regions consists of two consecutive anodic steps. All these events give an indication for the better resolution power of HCO_3^- ions in the anodic reaction over the whole potential range. This implies modification of the surface films or variation in chemical composition of the solution, which facilitate the next anodic step.

To probe the mechanisms, and for the sake of simplicity, each of the above four potential regions will be interpreted separately paying particular attention to HCO_3^- ions in the overall anodic process. Specific effects of OH^- ions produced from the hydrolysis of $NaHCO_3$ should also be taken into consideration.

3.5.1.1. *The active region (shoulder B and peak C)*. The anodic shoulder B appeared after hydrogen evolution and therefore may be attributed to the oxidation of adsorbed and even absorbed hydrogen atoms formed during the pre-cathodization of the electrode surface. In this regard it is informative to note correspondence between shoulder B and the cathodic peak M (Figure 3a), which coincide with the first stage of oxide formation. Thus, shoulder B may be attributed to the formation of $Fe(OH)_{ads}$ according to

$$Fe + OH^- = Fe(OH)_{ads} + e \quad (1)$$

Subsequently, the first anodic peak C should, in principal, correspond to the formation of a hydrous ferrous hydroxide layer, likely produced according to

$$Fe(OH)_{ads} + OH^- = Fe(OH)_2 + e \quad (2)$$

As suggested from the potential excursion studies, presented above, some dissolution of the $Fe(OH)_2$ surface film took place. This is explained as partial removal of $Fe(OH)_2$ by means of chemical dissolution, assisted by OH^- and/or HCO_3^- ions, as follows:

$$Fe(OH)_2 + OH^- = Fe(OH)_3^- \quad (3)$$

$$Fe(OH)_2 + HCO_3^- = CO_3^{2-} + OH^- + Fe^{2+} + H_2O \quad (4)$$

3.5.1.2. *The pre-passive region (peaks D and E)*. According to thermodynamic data, processes taking place in the potential region of anodic peak D may be attributed to the formation of Fe^{2+} species, most probably in the form of $Fe(OH)_2$ surface film. The reactions responsible for the formation of $Fe(OH)_2$ may be written as

$$Fe(OH)_{ads} + H_2O = Fe(OH)_{2ads} + H^+ + e \quad (5)$$

$$Fe(OH)_{2ads} + OH^- = HFeO_2^- + H_2O \quad (6)$$

$$HFeO_2^- + OH^- = FeO_2^{2-} + H_2O \quad (7)$$

$$HFeO_2^- + H_2O = Fe(OH)_2 + OH^- \quad (8)$$

Here, $HFeO_2^-$ is considered as the primary stable product of the electrode reaction and $Fe(OH)_2$ is considered as the final product. As such, the presence of $HFeO_2^-$ may be conceived to produce an inhibiting effect. On the other hand, $Fe(OH)_{2ads}$ could be taken as a possible reaction intermediate that is different from $Fe(OH)_2$. The latter might have emerged as a result of the local increase in $HFeO_2^-$ concentration. Also, the presence of HCO_3^- might have facilitated chemical dissolution of the outermost layer of $Fe(OH)_2$. Consequently, peak D may be assigned to the electroformation of $Fe(OH)_2$ surface film according to Equations 5, 6 and 8.

On the other hand, the presence of HCO_3^- ions causes precipitation of Fe^{2+} ions resulting from the dissolution of $Fe(OH)_2$. Once supersaturation of $FeCO_3$ is reached, precipitation of $FeCO_3$ takes place according to

$$HCO_3^- = CO_3^{2-} + H^+ \quad (9)$$

$$Fe^{2+} + CO_3^{2-} = FeCO_3 \quad (10)$$

It follows that peak E may be attributed to the formation of a film which is a mixture of an inner $Fe(OH)_2$ layer and an outer $FeCO_3$ layer.

However, $FeCO_3$ may be removed from the metal surface by two alternative means. The first is through the partial detachment of the complex pre-passive layer from the metal surface and the second may be assisted by chemical dissolution according to the following equations:

$$FeCO_3 + HCO_3^- = Fe(CO_3)_2^{2-} + H^+ \quad (11)$$

$$FeCO_3 + H^+ = Fe^{2+} + HCO_3^- \quad (12)$$

Following the above discussion, the pre-passive region can be ascribed to electrochemical dissolution of the electrode surface and formation of the same final product (i.e. $Fe(OH)_2$) through soluble intermediates such as $HFeO_2^-$ and FeO_2^{2-}, which contribute to the thickening of the anodic layer.

3.5.1.3. *The passive region (peak F and plateau G)*. The passive region is characterized by two consecutive stages (peak F and plateau G) separated by a definite potential (+0.25 V). Earlier investigators [20, 21] have found it convenient to interpret their experimental passive-state

data of iron and steel in alkaline media on the assumption of two region-passive states. However, it should be pointed out that the present study (see Figure 1) is the first which presents experimental evidence that the passive region under the prevailing experimental conditions consists of two well defined stages namely: peak F and plateau G.

Peak F is observed in the potential range −0.33 to +0.25 V, in which a higher valency oxide is expected to form, most probably, Fe_3O_4 surface film. Thus, peak F can be attributed to the formation of Fe_3O_4 surface film according to the following overall electrochemical reaction:

$$Fe + 2Fe(OH)_2 + 4OH^- = Fe_3O_4 + 4H_2O + 4e \quad (13)$$

The plateau G begins at a potential of +0.25 V, which is recognized as the 'critical passivation potential'. In order to elucidate the mechanism of passivation along plateau G, it is essential to understand the significance of the critical passivation potential (+0.250 V). At this critical potential, which is probably close to the potential of complete passivation, an oxygen-rich iron oxide is assumed to form as a passive film. Under these conditions, the oxygen in the water may transform Fe_3O_4 into a higher oxide, i.e., γ-Fe_2O_3. The latter possesses more effective passivating properties. Thus, at the critical passivation potential, the system may be pictured as being $Fe/Fe_3O_4/\gamma$-Fe_2O_3/H_2O and this explains the critical passivation potential as the equilibrium potential described by the reaction:

$$2Fe_3O_4 + H_2O = 3\gamma\text{-}Fe_2O_3 + 2H^+ + 2e \quad (14)$$

Here, attention is drawn to the experiment observation that no further change is noted during plateau G. This indicates that no further change in composition of the passive layer took place as it continued to thicken. In general, the field strength across the passive layer is expected to drive thickening of the passive film. If it is assumed that the interior part of the oxide layer (i.e. Fe_3O_4) is a good electronic conductor, the passive carbon steel would behave basically as an electrode system Fe/γ-Fe_2O_3/Fe^{2+}, H_2O. The equilibrium potential of the net reaction may be described by:

$$2Fe^{2+} + 3H_2O = \gamma\text{-}Fe_2O_3 + 6H^+ + 2e \quad (15)$$

It is generally recognized that the structures of the two oxides Fe_3O_4 and γ-Fe_2O_3 are closely related. The major difference between these two oxides is a pronounced difference in their electrical conductivity; the Fe_3O_4 inner layer is known to be a better conductor than the γ-Fe_2O_3 outer layer. Thus, the passivating layer formed during plateau G is believed to exhibit good protective properties.

Following the above discussion, the proposed structure and composition of the passive film formed on carbon steel in deaerated 0.50 M $NaHCO_3$ solution is illustrated in Figure 6. Both layers are porous but each retains a different structure-property pattern. It is not unreasonable to suggest that each layer maintains centrally located pores, and that the pores of γ-Fe_2O_3 do not necessarily extend to the metal surface. A passive layer with two-dimensional porosity must have been transformed to a three-dimensional nonporous oxide at steady state stoichiometry.

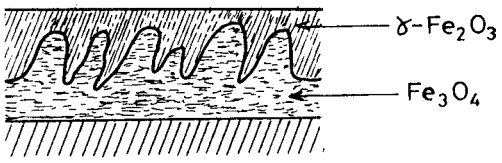

Fig. 6. Schematic illustration of the two oxide phases Fe_3O_4 /γ-Fe_2O_3 in the passive film.

3.5.1.4. *The trans-passive region (peak H and oxygen evolution)*. At potential +0.88 V and after complete passivation of the electrode surface, the electrode was noted to turn brownish red, with no evidence of continuous oxide phase as the electrode surface dissolves. The rather marked anodic step, prior to the steeply rising oxygen evolution branch, has been attributed to the generation of ferrate(VI) species [3, 10] according to the following overall reaction:

$$Fe + 4OH^- = FeO_4^{2-} + 4H^+ + 6e \quad (16)$$

Thus, peak (H), which was observed for the first time, has been associated with FeO_4^{2-} species.

The presence of HCO_3^- ions is believed to bring about the appearance of the anodic current peak H at a pH value lower than previously observed in alkaline solution of NaOH [3, 8]. The lowered pH may also serve to discern the processes corresponding to the formation of FeO_4^{2-} species and oxygen evolution. This demonstrates that OH^- ion concentration must have contributed considerably to the production of FeO_4^{2-} species. Apart from their electrochemical dissolution, the HCO_3^- ions are also thought to affect the solubility of the passivating film. Basically, this outcome may be related to the decreasing stability of the passivating film (γ-Fe_2O_3) in the presence of HCO_3^- ions.

However, the FeO_4^{2-} species can undergo two competitive chemical transformations, namely, the splitting off of oxygen via a redox catalysis mechanism and hydrolysis to yield free FeO_4^{2-} ions, which diffuse into the bulk solution [3].

3.5.2. *Cathodic reduction*

The first cathodic response is taken as a qualitative measure for the accumulation of FeO_4^{2-} species on the electrode surface. The influence of negative potential scan reversal shows that the normally expected first ferrate(VI) – reduction to Fe(III) was not observed.

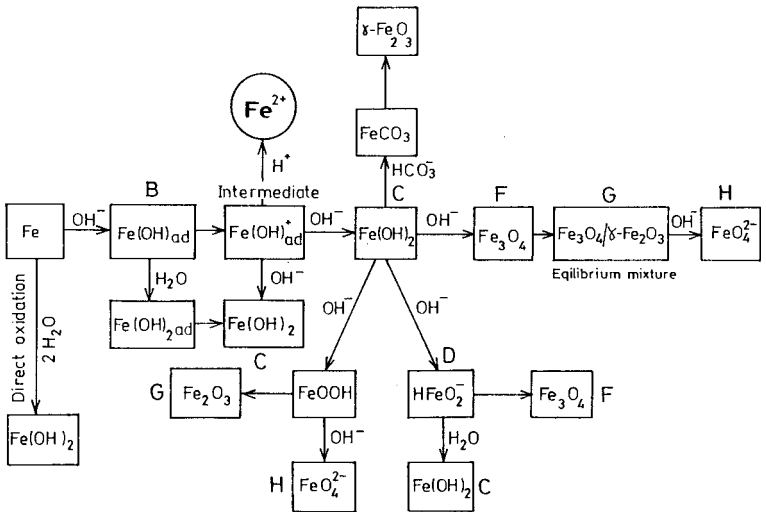

Fig. 7. Steps and their interrelations for the possible electrochemical oxidation and chemical dissolution of carbon steel in deareated 0.50 M $NaHCO_3$ solution.

Table 1. General characteristics of the four regions obtained from the cyclic voltammogram of carbon steel in deaerated 0.50 M $NaHCO_3$ solution (see Figure 1)

Region	Fe^{2+} species				Fe^{3+} species		Fe^{6+} species
	First region (active region)		Second region (pre-passive region)		Third region (passive region)		Fourth region (trans-passive region)
Stage	Shoulder B	Peak C	Peak D	Peak E	Peak F	Plateau G	Peak H, O_2 evolution
Pot. range /V, SCE	−0.91 to −0.79	−0.79 to −0.63	−0.63 to −0.50	−0.50 to −0.33	−0.33 to 0.25	0.25–0.88	0.88–1.25
Surface film	$Fe(OH)_{ad}$	Fe^{2+} $Fe(OH)_2$	$HFeO_2^-$	FeO_2^{2-} $Fe(OH)_2$	FeO_2^- Fe_3O_4	Composite layer Fe_3O_4/γ-Fe_2O_3	FeO_4^{2-}

Instead, electrochemical re-activation of the oxidation process related to peak H was observed (plateau J). This indicates that the oxygen evolution and formation of free ferrate(VI) ions were both chemical reactions starting from FeO_4^{2-} species at the electrode surface and that a surface in a lower oxidation-state (i.e. Fe_3O_4) has been left behind. Relevant studies [3, 22] support the absence of γ-Fe_2O_3 and the presence of Fe_3O_4 in the trans-passive stage.

On the other hand, the appearance of the first cathodic peak K is attributed to the reduction of Fe^{3+} species, i.e., the transformation of the Fe_3O_4 into Fe^{2+} species. Further reduction of Fe^{2+} species into Fe could take place through two reduction steps along shoulder L and peak M as evident from the potential excursion studies.

From the foregoing discussion, it is possible to summarize the various steps and their interrelations (Figure 7) for the anodic reactions of carbon steel in deaerated 0.50 M $NaHCO_3$ solution of pH 8.72.

4. Conclusions

The electrochemical characteristics of carbon steel in deaerated $NaHCO_3$ solution at pH 8.72 may be explained through a series of successive reactions primarily involving the formation of $Fe(OH)_{ads}$, $Fe(OH)_2$, Fe_3O_4, Fe_3O_4/γ-Fe_2O_3, FeO_4^{2-} and finally oxygen evolution.

Examination of the cyclic voltammograms and the electrode surface response during the negatively directed potential excursions revealed that:

(i) In the negative potential region of the forward anodic branch (before passivation), carbon steel surface appeared like blank metal, which gave rise to small current densities accompanied by the formation of a thin surface film.

(ii) After pre-passivation (i.e. in the positive potential region), the electrode surface became brown red and a relatively high current density was noticed.

(iii) In the more positive potential region (i.e. trans-passive region), no oxide phase was formed on the electrode surface but the formation of Fe^{6+} species in solution was deduced.

References

1. E. Castro, C. Valentini, C. Moina, J. Vilche and A.J. Arvia, *Corros. Sci.* **26** (1986) 781.

2. C. Valentini, C. Moina, J. Vilche and A.J. Arvia, *Corros. Sci.* **25** (1985) 985.
3. F. Beck, R. Kauss and M. Oberst, *Electrochim. Acta* **30** (1985) 173.
4. F. Clerbois and J. Massart, *Corros. Sci.* **2** (1962) 1.
5. D. Gilroy and J.E.O. Mayne, *Br. Corr. J.* **1** (1966) 161.
6. J. Thomas, T. Nurse and R. Walker, *Br. Corr. J.* **5** (1970) 85.
7. R. Armstrong and A. Coates, *J. Electroanal. Chem.* **50** (1974) 303.
8. R. Guzman, J. Vilche and A.J. Arvia, *Electrochim. Acta* **24** (1978) 395.
9. D. Davies and J. Burstein, *Corrosion* **36** (1980) 416.
10. C. Rangel, I. Fonseca and R. Leitao, *Electrochim. Acta* **31** (1986) 1659.
11. H. Silver and E. Lekas, *J. Electrochem. Soc.* **117** (1970) 5.
12. I. Geronov, T. Tomov and S. Georgiev, *J. Appl. Electrochem.* **5** (1975) 351.
13. L. Ojefors, *J. Electrochem. Soc.* **123** (1976) 1691.
14. J. Rubim and J. Dunnwald, *J. Electroanal. Chem.* **258** (1989) 327.
15 J. Gui and T.M. Devine, *Corros. Sci.* **37** (1995) 1177.
16. E. Martini and I.L. Muller, *Corros. Sci.* **42** (2000) 443.
17. W.J. Lorenz and K. Heusler, in F. Mansfeld (ed.), 'Corrosion Mechanisms', (Marcel Dekker, Inc., New York, 1987), pp. 1–84.
18. W. Baek, T. Kang, H. Sohn and Y. Kho, *Electrochim. Acta* **46** (2001) 2321.
19. J. Park, S. Pyun, J. Lee and H. Kim, *Corrosion* **55** (1999) 380.
20. D. Geana, A. EL-Miligy and W.J. Lorenz, *J. Appl. Electrochem.* **4** (1974) 337.
21. N. Sato, K. Kudo and R. Nishimura, *J. Electrochem. Soc.* **123** (1976) 1419.
22. C. Foley, J. Kruger and C. Bechtold, *J. Electrochem. Soc.* **114** (1967) 994.